6C.5 ON THE GENESIS OF TROPICAL STORM EUGENE (2005) ASSOCIATED WITH THE ITCZ BREAKDOWNS

Chanh Q. Kieu, and Da-Lin Zhang
Department of Atmospheric and Oceanic Science, University of Maryland
College Park, MD 20742

1. Introduction

Despite considerable progress in the forecasts of tropical cyclone (TC) track and intensity during the past few decades, tropical cyclone genesis (TCG), a process by which a weak atmospheric disturbance grows into a tropical storm (TS), still remains elusive due partly to the lack of high-resolution observations at the very early stage of TCG and partly to the deficiencies in current TC models. There are numerous disturbances of different scales but only a small percentage could develop into TCs (e.g., McBride and Zehr 1981; DeMaria 2001). Many processes leading to TCG are well known but they remain poorly understood. In particular, we are still searching for the mechanisms by which the surface circulations could be spun up to initiate the wind-induced surface heat exchange (WISHE) process as a route to TSs.

The bottom-up and top-down hypotheses have been proposed recently as two of the possible processes leading to TCG from midlevel mesoscale convective vortices (MCVs) associated with mesoscale convective systems (MCSs). Specifically, Zhang and Bao (1996a,b) find that an MCV provides the necessary quasi-balanced forcing for the initiation and organization of (parameterized) deep convection, and that it is deep convection that contributes to the amplification of the low-level cyclonic vorticity through stretching in the presence of intensifying flows. This bottom-up mechanism was later advanced by cloud-resolving studies of Hendricks et al. (2004) and Montgomery et al. (2006), in which the concept of convective "hot towers" proposed by Riehl and Malkus (1958) was extended to that of "vortical hot towers (VHTs)". In this bottom-up hypothesis, Montgomery and Enagonio (1998) treat TCG as a result of the mean–eddy interaction, the so-called axisymmetrization. In contrast, the top-down hypotheses deal with two different scenarios: one is related to the merging dynamics of midlevel MCVs within a larger-scale low-level cyclonic circulation (Ritchie and Holland 1997, hereafter RH97; Simpson et al. 1997) whereas the other focuses more on the thermodynamics of a single MCV (Bister and Emanuel 1997).

A recent statistical study of TCG over the Eastern Pacific during the active seasons of 1999-2003 shows that most of the TCG events in the this ocean basin are associated with the Intertropical Convergence Zone (ITCZ) breakdowns caused by easterly propagating tropical disturbances (Wang and Magnusdottir 2006, hereafter WM06). While the ITCZ breakdowns could be attributed to the internal dynamical instability, the so-called roll-up mechanism discussed by Nieto Ferreira and Schubert (1997), WM06's study appears to suggest that merging MCVs associated with the ITCZ breakdowns are efficient in initiating the TCG processes.

The objectives of the present study are to (a) present the kinematics of the vortex merger and the associated multiscale features; and (b) examine quantitatively how merger of the two midlevel MCVs could account for the formation of TS Eugene (2005) through the PV and vorticity budgets. These objectives will be achieved using a 4-day cloud-resolving simulation of TS Eugene during NASA's field campaign of the Tropical Cloud Systems and Processes (TCSP; see Halverson et al. 2007) with the Weather Research and Forecast (WRF) model (Kieu and Zhang 2008).

Achieving the above objectives can help understand how the low-level cyclonic circulation grows in the presence of midlevel MCVs from either the bottom upward or top downward.

2. Vortex merging kinematics

Fig. 1 shows the evolution of the simulated maximal surface wind and minimum sea level pressure, which indicates that Eugene's life cycle can be divided into four phases: a pre-genesis phase with a slow evolution prior to 0600 UTC 18 July or 30 h into the simulation (hereafter referred to as 18/06-30), a vortex-merging genesis phase from 18/06-30 to 18/15-39, a WISHE-deepening phase from 18/15-39 to 19/15-63, and a decaying phase afterwards. The first is characterized by a loosely defined ITCZ trough with trade winds from both hemispheres, and the second by closed isobars with the maximum surface wind exceeding 18 m s^{-1} - a threshold for a TS. Eugene is a weak storm with the maximum surface wind slightly above the threshold for a hurricane.

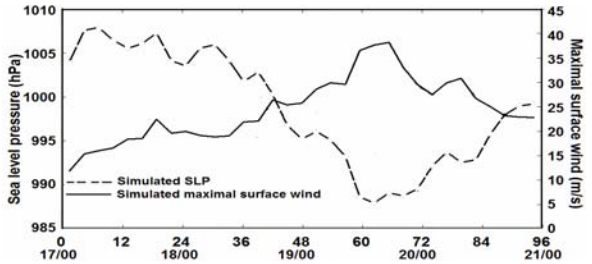

Figure 1. Time series of the simulated maximum surface wind (solid, m s^{-1}) and minimum sea-level pressure (dashed, hPa) during the 4-day period of 17/00-00 to 21/00-96.

Of interest, the genesis of Eugene is marked noticeably by the merger of two mesovortices V_1 and V_2 that were spawned within the ITCZ about 10 days before the model initialization. The merger is visible from GOES satellite images, NCEP $1^0 \times 1^0$ reanalysis, and the model simulation. Fig. 2 shows the east-west vertical cross sections of the longitudionally averaged PV and its local tendencies from the WRF simulation during the merging period. It is evident that the merger is not a simple capture of V_1 by V_2. The two MCVs consist of many meso-γ scale PV entities or vortices, and the MCV-merging process is characterized by the gradual capture of each of the γ-scale vortices within the quasi-stationary V_2 by the northwestward propagating V_1.

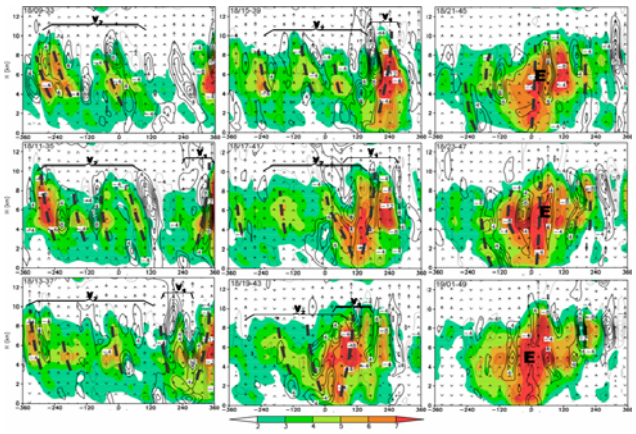

Figure 2. Vertical cross sections along the line connecting V_1-V_2 centers of the total PV integrated +/- 360 km along the south-north direction (shading, unit of 1 PVU), and the corresponding integrated PV tendency (contour, unit of 10^{-4} PVU s^{-1}) valid from 18/09-33 to 19/01-49. Bold dashed lines are for the mesovortices spawn within V_2 and V_1 during merging period. Superimposed is the vertical motion (vectors)

V_2 becomes more fragmented and slowly elongated along the sheared flows before wrapping around V_1 as the cyclonic circulation increases. It should be mentioned that due to the smaller size, V_1's circulations at individual levels are seen being absorbed by V_2's as V_1 coalescences and enters the northern half portion of V_2's circulation (Fig. 3). So, V_1 may be viewed in three-dimension (3D) context as a "comma head" that rolls up with V_2's PV-containing vortices in the tail (Fig. 3). No mutual rotation around a common center is observed.

Of particular relevance to this study is a significant increase in intensity and 3D volume of PV as V_1 captures each γ-scale vortex after 18/15-39. This increase is remarkably pronounced in the midtroposphere where the

peak PV associated with most of the γ-scale vortices is located. By 18/23-47, a robust vortex-merger emerges with higher-PV concentration but a smaller circulation size; namely, the west-east width of the merger has shrunk by half during the past 10 h (i.e., 18/13-37 to 18/23-47). Clearly, the shrunk size, and the increased PV amplitude and volume caused by the vortex merging are all favorable for the deepening of the surface cyclone (Fig. 1)

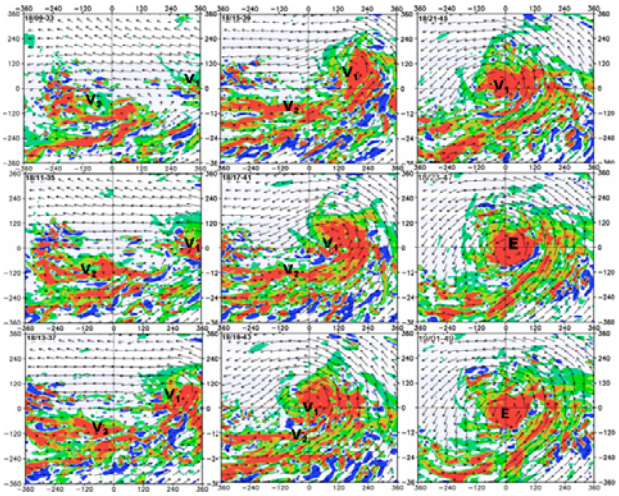

Figure 3. Horizontal distributions of the vertically mass-weighted PV (shaded, intervals of 0.2 PVU) superimposed by the flow field at z = 3 km (vectors) during the merging periods from 18/09-33 to 18/23-47.

In the next section, some internal dynamical processes besides the PV fluxes will be shown to contribute effectively to the increase of the total PV within the control volume.

3. Merging dynamics

a. PV budget analysis

We have seen above the significant local increase of PV near the vortex center and the increased high-PV volume during the vortex-merging period. This increase has been noticed in previous idealized study by RH97 but little quantitative explanations have been provided. In this section, we attempt to gain insight into the dynamical processes that account for this increase of the total PV (VPV) through the PV budget analysis, and then relate the increased midlevel PV to the surface genesis of Eugene.

Because any physical system always occupies a finite volume, the PV equation has to be re-formulated in the integral form to take into account this finite volume before any budget analysis is performed. In the integral form, the PV equation is given by:

$$\frac{d}{dt}\left(\int_{V(t)} qdV\right) = \int_{V(t)} (q\nabla \bullet \vec{u})dV + \int_{V(t)} \frac{\vec{\omega} \bullet \nabla H}{\rho} dV + \int_{V(t)} \frac{\nabla \bullet (\vec{F} \times \nabla \theta)}{\rho} dV + \int_{S(t)} q(\vec{U} - \vec{u}) \bullet \vec{n} dS \quad (1)$$

Eq. (1) states that the time rate of VPV changes (QTEN) is determined by the terms on its rhs, which are from left to right the condensing or diluting rate of PV due to the 3D velocity divergence (QCON), the dot product of the 3D absolute vorticity and the 3D diabatic heating gradient (QH, hereafter referred to as the diabatic-PV production rate), the divergence of $\vec{F} \times \nabla\theta$, and the net across-boundary PV fluxes (QBND) consisting of the 3D normal-to-boundary flows (QFLX) and the control volume's movement (QMOV). Note that the 3D divergence is proportional to minus of the time rate of density changes (i.e., -d($ln\rho$)/dt). So, QCON is ultimately connected to the mass exchange of the control volume with the surrounding environment. To characterize the system by VPV, we will weight Eq. (1) with the total volume and consider this equation as the governing equation for the mean PV associated with the vortex along its track.

It is evident from Fig. 4a that the VPV associated with V_2 increases slowly prior to merger (i.e., 18/06-30), moderate to sharply during its merging with V_1 (i.e., from 18/12-30 to 18/18-42), steadily until Eugene reaches its maximum intensity at 19/15-63, and decreases slowly shortly after; these sequences correspond well to the aforementioned four phases of Eugene's life cycle (cf. Figs. 4a and 1).

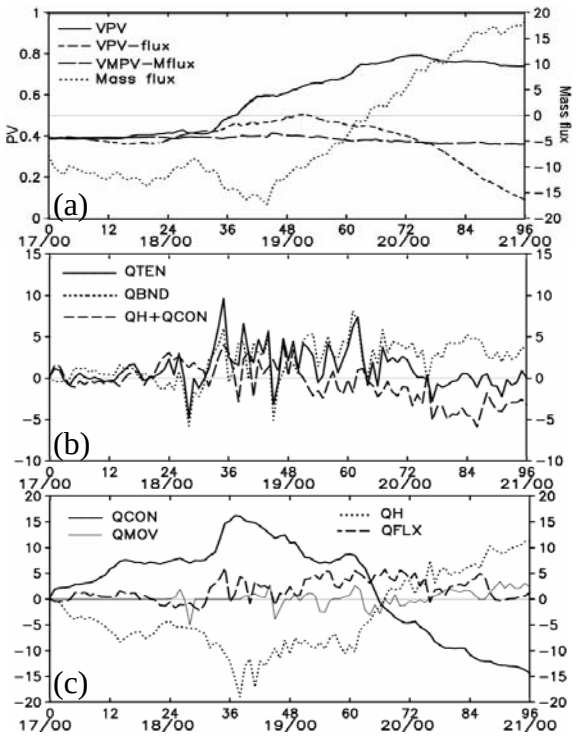

Figure 4. Time series of (a) VPV (solid, unit: PVU), VPV after subtracted net PV flux (short-dashed), MVPV after subtracted net MWPV flux at the boundaries (long-dashed), and total mass flux (dotted, unit: 10^7 kg s^{-1}); (b) the total VPV tendency (solid), the net PV fluxes (dotted), and the summation of the PV condensing and heating-generation rates (dashed); and (c) the PV condensing rate (solid), the PV generation rate by diabatic heating (dashed), the PV boundary flux due to normal flows (dotted), and the movement of the control volume (thin solid). The unit in (b) and (c) is 10^{-6} PVU s^{-1}. The time series are calculated for a control volume of 720 km × 720 km × 10 km that is fixed at the V_2 center from 17/00-00 to 18/18-42 and follow the Eugene center thereafter. All time series are normalized by the total volume.

As seen in Fig. 4a, VPV doubles its magnitude, i.e., from 0.4 to 0.8 PVUs, in about 40 h, and this increase coincides well with the amplification of Eugene during and after the merging phase (cf. Fig. 2). The increase of VPV is due to the contributions from the PV fluxes (i.e., the surface integrals on the rhs of Eq. (1)) together with the internal dynamics within the volume (i.e., the volume integrals on the rhs of Eq. (1)). It is important that about 50% of the increased VPV during the merging period is generated by internal dynamics, as seen after subtracting the PV fluxes from the total PV forcing (short-dashed line in Fig. 4a). The same budget calculation for the total mass-weighted PV (VMPV) shows that there is no similar internal forcing for the VMPV as for VPV, and the flux accounts completely for the changes of the VMPV with time (long dashed-line in Fig. 4a).

Fig. 4c reveals that the two dominant forcing terms in the VPV budget calculation QCON and QH are similar in magnitude but opposite in sign: QCON is a source (sink) when the mass in the control volume decreases (increases) whereas QH is a sink (source) when more convective (stratiform) heating occurs during the intensifying (weakening) stage. Note that QCON is peaked shortly after 18/12-36, when more midlevel PV entities of V_2 are rolled up by V_1; this also coincides with the sharp increase in VPV. After reaching the maximum intensity of Eugene, QCON switches to a negative sign, i.e., the dilution of PV as a result of the inward mass flux into the control volume (Fig. 4a), whereas QH changes to a positive sign as stratiform rainfall with an upper-level heating maximum dominates over convective rainfall. Although the negative net forcing (QCON + QH) after 19/03-51 occurs after a brief period of dissipation, Eugene still experiences another deepening period, i.e., from 19/03-51 to 19/15-63 (cf. Figs. 4b and 1), due to the continued supply of high PV from the ITCZ. This implies that without the contribution of QBND, Eugene would become shorter-lived under the influence of vertical wind shear. During the decaying phase, QCON is more or less balanced with QBND and QH (Figs. 4b,c).

The negative contribution of diabatic heating (QH) to the VPV production during the intensifying stage appears to contradict our common intuition. To provide some explanations for the subtle contribution of QH, Fig. 5 show the vertical profile of (area-averaged) density, diabatic heating, velocity divergence and rotations during the three different phases.

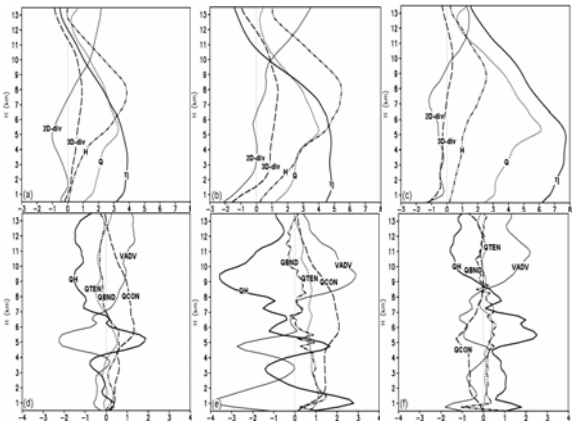

Figure 5. Vertical profiles of the area average of (a), (b), and (c) the absolute vorticity (solid, unit: 10^{-5} s^{-1}), PV (dotted, unit: 0.2 PVU), the 3D divergence (dashed, unit: 10^{-5} s^{-1}), diabatic heating (dot-dashed, unit: 0.2×10^{-3} K s^{-1}), and 2D divergence (thin solid, unit: 10^{-5} s^{-1}); and (c), (d) and (f) PV generation rates by diabatic heating (solid), PV condensing rates (dashed), the lateral PV fluxes (dot-dashed), mean vertical advection $-\partial(wQ)/\partial z$ (thin solid) and the total PV rates (dotted) for three different times: 18/03-27 (left panel), and 18/12-36 (middle panel) and 20/00-72 (right panel). Unit in (d)-(f) is 10^{-5} PVU s^{-1}

The contribution to QH, viewed in the cylindrical coordinate, comes from two sources: the radial and the vertical parts. The radial component of QH [i.e., $(\omega_r \partial H/\partial r)/\rho$ where ω_r is the radial component of the absolute vorticity] that is often neglected is largely negative (positive) in the lower (upper) troposphere for any hurricane-like vortex. In contrast, the vertical component of QH, i.e., $(\eta \partial H/\partial z)/\rho$, show dual positive peaks below the maximal heating level, where η is the vertical component of absolute vorticity (Figs. 5a-5c). The total contributions from the vertical and radial parts of QH result in the diabatic-PV generation and destruction in the lower and upper troposphere, respectively. Given the fact that air density decreases exponentially with height, a skewed vertical distribution of $(\eta \partial H/\partial z)/\rho$ would result, with a larger magnitude near the top of the PBL. This is illustrated by smaller vertically-integrated PV generation rates in the lower troposphere than vertically integrated PV destruction rates in the upper troposphere (Figs. 5d-f), yielding the net negative diabatic contribution to QTEN during the intensifying stage.

By comparison, positive QCON appears in the deep troposphere with its peak in the 5 – 6 km layer during the intensifying stage (see Figs. 5d, e); the peak of QCON coincides with that of PV, providing direct evidence of its role in intensifying PV and TCG. Clearly, as long as the total mass in the volume keeps decreasing, the VPV and TC would continue to intensify through QCON. It is apparent that the intensify stage (i.e., from 18/00-24 to 19/03-51) is characterized with positive net contributions of QCON and QH, representing the internal dynamical processes, to the VPV time series (Fig. 5a). Their net effects are to increase PV in the lower half of the troposphere and decrease it aloft, but at a much higher rate in the former, during the merging phase (Figs. 5d, e).

b. Bottom-up vorticity generation

One remarkable contrast between the vertical component of the absolute vorticity (η) and PV is that η experiences the most rapid increase in the lower half of the troposphere during the merging phase, with upright η-isopleths from the peak PV level down to the surface (Fig. 6).

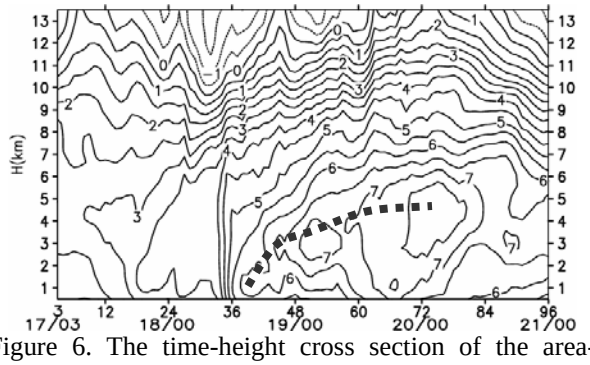

Figure 6. The time-height cross section of the area-average of (a) vertical component of the absolute vorticity (solid, intervals of 10^{-5} s^{-1}) and stretching (shaded, intervals of 5×10^{-10} s^{-2}). Bold dashed line denotes vorticity maxima.

This result seems not imply the

downward development of the midlevel cyclonic vorticity, as hypothesized by RH97. In fact, the vortex merging leads to positive local vorticity tendencies in the deep troposphere, but with the maximum value in the PBL.

To gain some insights into the bottom-up development of cyclonic vorticity, we now look at the budget calculation for the absolute vorticity in the flux form (Haynes and McIntyre 1987).

$$\frac{\partial \eta}{\partial t} = -\frac{\partial}{\partial x}\left(u\eta + w\frac{\partial v}{\partial z} - F_y\right) - \frac{\partial}{\partial y}\left(v\eta - \frac{\partial u}{\partial z} + F_x\right) + SOL$$

$$= -\left[\frac{\partial (u\eta)}{\partial x} + \frac{\partial (v\eta)}{\partial y}\right] - \left[\frac{\partial}{\partial x}\left(w\frac{\partial v}{\partial z}\right) - \frac{\partial}{\partial y}\left(w\frac{\partial u}{\partial z}\right)\right] \quad (2)$$

$$+ \left[\frac{\partial F_y}{\partial x} - \frac{\partial F_x}{\partial y}\right] + SOL$$

where the rhs of Eq. (2) is grouped in the form such that the first two terms correspond to the stretching and tilting forcings of the material vorticity equation. These are two dominant terms and, upon taking volume integration, represent respectively the vorticity flux at the lateral boundary (or volume stretching, hereafter VSTR) and the change of the circulation area projected onto the horizontal plane (or volume tilting, hereafter VTIL).

As seen in Fig. 7, the upward growth of vorticity in Fig. 6 is attributed mainly to VSTR in the presence of convergence up to the peak heating level. Apparently, VSTR is peaked in the PBL, with a secondary maximum near the melting level. If the cyclonic vorticity grows downward, one would expect the occurrence of higher local tendencies below the level of high PV. Instead, Fig. 7a shows that the amplitude of cyclonic vorticity grows, after the merger, from the bottom upward to about 4 km at 20/03-75.

The low-level maximum of VSTR is obvious from a well-known fact of the dominant low-level convergence. However, re-called here that since PV is considered as the dynamical variable, the absolute vorticity as well as 3D flows are now diagnostic variables. These diagnostic variables are the balanced flows associated with a given PV distribution. The question of how the midlevel increased PV can help promote the upward growth of vorticity should not be, therefore, relied on the *given* low-level stretching.

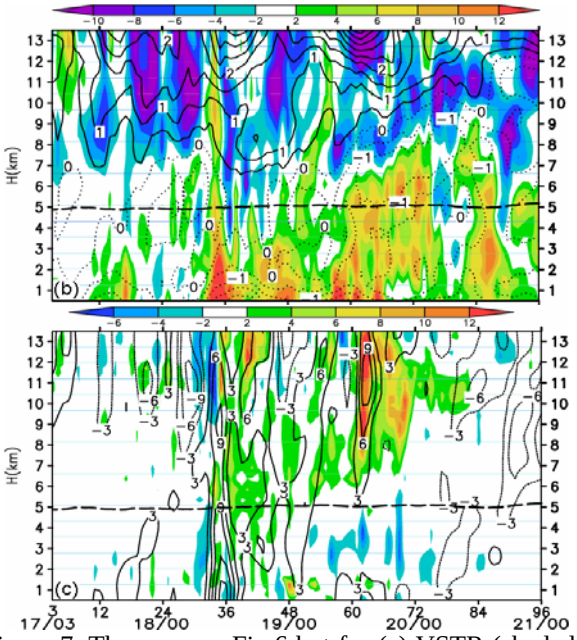

Figure 7. The same as Fig.6 but for (a) VSTR (shaded, intervals of 1×10^{-10} s^{-2}) and 2D divergence (contour, intervals of 10^{-5} s^{-1}); and (b) VTIL (shaded, intervals of 1×10^{-10} s^{-2}) and the tendency of the absolute vorticity from the model evaluated from hourly output (solid, contoured of 3×10^{-10} s^{-2}). Dashed line denotes the melting level.

In fact, the roles of PV in triggering the bottom-up development of vorticity have to be answered from the point of view of the balanced dynamics. As the PV at the midlevel increases, both mass and flow fields will adjust to the new PV distribution according to the invertibility principle (Hoskins et al. 1985). This adjustment takes place thorough the column, leading to the maximal deformation of the isobaric surfaces at the lowest levels, especially in the presence of the warm core from low- to-mid- levels. As a result of the balanced constraint, vorticity will be strengthened near the surface in accord with the development of the minimum surface

pressure and this is what is seen in Fig. 6 after 18/12-36. A further examination of the quasi-balanced PV-omega system (cf. e.g., Zhang and Bao 2004) will show further the existence of the maximal low-level convergence near the surface, which explains for the peak of VSTR from z = 0 – 3 km as seen in Fig. 7a.

4. Concluding remarks

In this study, the cyclogenesis of TS Eugene (2005) from the vortex merger is examined, using the cloud-resolving simulation with the WRF model. We have demonstrated that the formation of Eugene was a result of a vortex-vortex interaction between two MCVs that might have originated from one of the ITCZ breakdown episodes. The vortex merger is not a simple capture of one by the other but is marked by the gradual capture of each of the γ-scale vortices within the quasi-stationary V_2 by the northwestward propagating V_1. Model results reveal particularly that the total PV increases sharply during the merging period in connection with the birth of Tropical Depression Eugene.

Budget calculation of the total PV within a control volume enclosing the MCVs shows that the increase of the total PV is due to 1) the continuous PV fluxes associated with the ITCZ and V_1 at the lateral boundaries, and 2) the internal dynamics within volume. The internal dynamics plays important roles in the increase of the total PV. As the volume losses its total mass to the ambient environment in response to the balanced adjustment, PV appears to be "concentrated" more within the volume. This accounts for about 50% of the net increase of PV within the volume during the merging period. Of another interest, the contributions from diabatic heating to the total PV are no longer simple. As the finite volume of the system is taken into account, diabatic heating now has some internal structure inside the volume, and the net contribution of diabatic heating (more precisely, of the 3D gradient of heating coupled with 3D rotation) is to decrease the total PV.

Under the constraint of the balanced dynamics, low-level vorticity is strengthened rapidly due to the adjustment of mass and flow fields to the increase of midlevel PV. The strengthening takes place most effectively at the lowest levels where the response of the mass and flow fields to the midlevel increased PV is most profound, and later expands upward.

REFERENCES

Bister, M., and K. A. Emanuel, 1997: The genesis of Hurricane Guillermo: TEXMEX analyses and a modeling study. *Mon. Wea. Rev.*, **125**, 2662–2682.

DeMaria, M., J.A. Knaff, and B.H. Connell, 2001: A tropical cyclone genesis parameter for the tropical Atlantic. *Wea. Forecasting*, **16**, 219–233.

Ferreira, R. N., and W. H. Schubert, 1997: Barotropic aspects of ITCZ breakdown. *J. Atmos. Sci.*, **54**, 261–285.

Halverson, J., M. Black, S. Braun, D. Cecil, M. Goodman, A. Heymsfield, G. Heymsfield, R. Hood, T. Krishnamurti, G. McFarquhar, M.J. Mahoney, J. Molinari, R. Rogers, J. Turk, C. Velden, D.-L. Zhang, E. Zipser, and R. Kakar, 2007: NASA's Tropical Cloud Systems and Processes Experiment. *Bull. Amer. Meteor. Soc.*, **88**, 867–882.

Haynes, P., and M. McIntyre, 1987: On the Evolution of Vorticity and Potential Vorticity in the Presence of Diabatic Heating and Frictional or Other Forces. *J. Atmos. Sci.*, **44**, 828–841.

Hendricks, E. A., M. T. Montgomery, and C. A. Davis, 2004: The role of "vortical" hot towers in the formation of tropical cyclone Diana (1984). *J. Atmos. Sci.*, **61**, 1209–1232.

Hoskins, B. J., M. E. McIntyre, and A. W. Robertson, 1985: On the use and significance of isentropic potential vorticity maps. *Quart. J. Roy. Meteor. Soc.*, **111**, 877–946.

Kieu, C. Q., and D. L. Zhang, 2008: Genesis of Tropical Storm Eugene (2005) associated with the ITCZ breakdowns. Part I: Observational and modeling analyses. *Submitted to J. Atmos. Sci*. (conditionally accepted).

McBride, J.L., and R. Zehr, 1981: Observational analysis of tropical cyclone formation. Part II: Comparison of non-developing versus developing systems. *J. Atmos. Sci.*, **38**, 1132–1151.

Montgomery, M. T, and J. Enagonio, 1998: Tropical cyclogenesis via convectively forced vortex Rossby

waves in a three-dimensional quasigeostrophic Model. *J. Atmos. Sci.*, **55**, 3176–3207.

___, M. E. Nicholls, T. A. Cram, and A. B. Saunders, 2006: A vortical hot tower route to tropical cyclogenesis. *J. Atmos. Sci.*, **63**, 355–386

Riehl, H., and J. S. Malkus, 1958: On the heat balance in the equatorial trough zone. *Geophysica*, **6**, 503-538.

Ritchie E. A., and G. J. Holland, 1997: Scale interactions during the formation of Typhoon Irving. *Mon. Wea. Rev.*, **125**, 1377–1396.

Simpson J., E. A. Ritchie, G. J. Holland, J. Halverson, and S. Stewart, 1997: Mesoscale interactions in tropical cyclone genesis. *Mon. Wea. Rev.*, **125**, 2643–2661.

Wang, C. C., and G. Magnusdottir, 2006: The ITCZ in the central and eastern Pacific on synoptic time scales. *Mon. Wea. Rev.*, **134**, 1405–1421.

Zhang, D. L., and N. Bao, 1996: Oceanic cyclogenesis as induced by a mesoscale convective system moving offshore. Part II: Genesis and thermodynamic transformation. *Mon. Wea. Rev.*, **124**, 2206–2226.